Steel and Composite Structures, *Vol. 30, No. 6 (2019) 577-589*
DOI: https://doi.org/10.12989/scs.2019.30.6.577

Vibration performance of composite steel-bar truss slab with steel girder

Jiepeng Liu [1,2a], Liang Cao [*1,2] and Y. Frank Chen [1,2b]

[1] *School of Civil Engineering, Chongqing University, Chongqing 400045, China*
[2] *Key Laboratory of New Technology for Construction of Cities in Mountain Area (Chongqing University), Ministry of Education, Chongqing 400045, China*

(*Received April 1, 2018, Revised February 21, 2019, Accepted March 12, 2019*)

Abstract. In this study, on-site testing was carried out to investigate the vibration performance of a composite steel-bar truss slab with steel girder system. Ambient vibration was performed to capture the primary vibration parameters (natural frequencies, damping ratios, and mode shapes). The composite floor possesses low frequency (< 10 Hz) and damping (< 2%). Based on experimental, theoretical, and numerical analyses on natural frequencies and mode shapes, the boundary condition of SCSC (i.e., two opposite edges simply-supported and the other two edges clamped) is deemed more reasonable for the composite floor. Walking excitations by one person (single excitation), two persons (dual excitation), and three persons (triple excitation) were considered to evaluate the vibration serviceability of the composite floor. The measured acceleration results show a satisfactory vibration perceptibility. For design convenience and safety, a crest factor β_{rp} describing the ratio of peak acceleration to root-mean-square acceleration induced from the walking excitations is proposed. The comparisons of the modal parameters determined by ambient vibration and walking tests reveal the interaction effect between the human excitation and the composite floor.

Keywords: steel-bar truss slab; composite floor; human-structure interaction; vibration serviceability; crest factor

1. Introduction

In recent years, the composite steel-concrete system has been widely used in buildings (Ferrer *et al*. 2018, Gou *et al*. 2018, Hadjioannou *et al*. 2018, Kataoka *et al*. 2017, Kimani and Kaewunruen 2017, Kyvelou *et al*. 2018, Quang *et al*. 2018, Wang 2005), infrastructures, footbridges (Gonilha *et al*. 2014), and bridges (Madrazo-Aguirre *et al*. 2015), as the longer span and lighter structural form has become a trendy design choice. The composite steel-bar truss slab (CSTS) with steel girder system shown in Fig. 1 is one kind of novel composite structures, which includes the slab consisting of a steel truss system (JG/T 368-2012 2012) with top, bottom and web reinforcing bars (Fig. 1(a)), baseplate, and steel girder (Fig. 1(b)).

In reviewing the relevant literature, the CSTS system has the following advantages (Colajanni *et al*. 2017, Wang *et al*. 2015, 2016, 2017b):

(1) Reasonable stress level and good economy;
(2) Suitable for long-span floor systems and convenient for construction;
(3) Reduction in construction time and labor cost; and
(4) Good crack and fire resistances.

Applications of the CSTS system can be extended to school buildings, movie theaters, prefabricated buildings, and industrial factories. Some issues concerning the static and dynamical performances of the CSTS system have been studied, including cracks and bearing capacity (Li *et al*. 2012), fire resistance (Wang *et al*. 2015), short-term rigidity (Cheng *et al*. 2013), structural failure (Huang *et al*. 2005), shear connection capacity (Colajanni *et al*. 2017), and seismic behavior (Wang *et al*. 2017a). However, it has been known that the design of a long-span and light structure (e.g., CSTS with steel girder) is often governed by a serviceability requirement rather than the strength one (Van Nimmen *et al*. 2017, Zhou *et al*. 2016). One of the important serviceability requirements is the acceptance/ perception of the vibration caused by human activities (Votsis *et al*. 2017, Nguyen *et al*. 2012) such as walking, running, and aerobics dancing, which should be considered to prevent the functionality of the structure from being compromised by excessive vibrations. This issue has not been fully understood for a CSTS with steel girder. Vibration serviceability problem may arise if the vibration amplitude is beyond a certain limit, annoying the occupants and affecting the vibration-sensitive equipment. Hence, a further investigation on human vibrations in the CSTS with steel girder is warranted. Specifically, the modal parameters and acceleration response were examined.

The objectives of this study are:

- To analyze the data measured from ambient vibration and then to ascertain the modal parameters and boundary conditions;
- To analyze the data measured from walking vibrations (including single, dual, and triple

*Corresponding author, Post-Doctor,
E-mail: liangcao@cqu.edu.cn
[a] Professor
[b] Professor

ISSN: 1229-9367 (Print), 1598-6233 (Online)

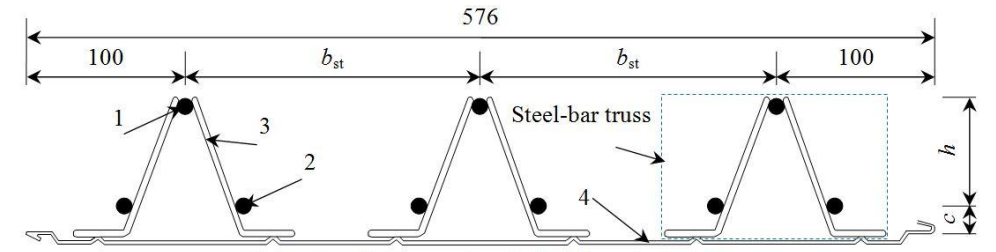

1: Top bar; 2: Bottom bar; 3: Web bar; 4: Baseplate
b_{st}: Distance between the adjacent steel-bar truss; c: Concrete cover thickness; h: Height of steel bar truss

(a) Cross section of the steel-bar truss slab

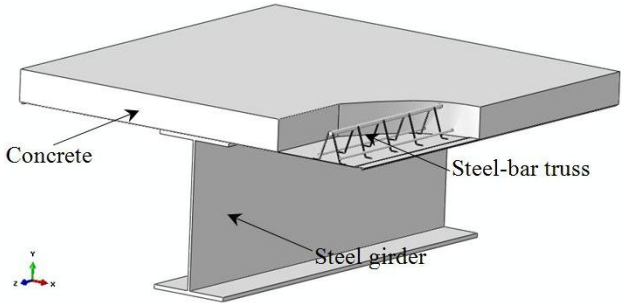

(b) Composite floor system

Fig. 1 Diagrams showing the composite steel-bar truss slab with steel girder (unit: mm)

excitations) and then to evaluate the vibration serviceability;
- To compare the modal parameters obtained from the ambient and walking vibrations and to verify the human-structure interaction effect;
- To propose the crest factor β_{rp} for calculating the root-mean-square (RMS) acceleration.

2. Description of prototype floor and accelerometer layout

In-situ test is a practical way to study the vibration performance of the CSTS with steel girder under human daily activities and to determine its dynamic properties (Chen *et al.* 2014, Fahmy and Sidky 2012). The investigated CSTS with steel girder in this study was intended to be used in meeting rooms, which locates in Yongchuan, Chongqing, China. The CSTS with steel girder had been designed to meet the usual building requirements including structural safely, fire resistance, and maximum deflection. The structural arrangement and cross section of the investigated composite floor is shown in Fig. 2, and the on-site view of the composite floor is shown in Fig. 3. The thickness and material specification for the steel-bar truss slab are listed in Table 1 and the detailed cross sections and yield strength for H-shaped steel girders are indicated in Table 2. The elasticity modulus of concrete is 3.00×10^4 MPa. The composite floor was completed prior to the installation of any nonstructural component (e.g., ceiling, duct, mechanical equipment, and partition).

Fig. 2(a) shows the schematic accelerometer locations along with a coordinate system used to obtain the dynamic characteristics and vertical acceleration response of the composite floor, where A_{ij} (i = 1-8, j = 1-9) represents the jth accelerometer location for the ith test. From the figure, it is known that 72 accelerometers would be needed for one-off measurement. However, the monitoring system used in this study consists of only ten accelerometers DH610V ranging ±5 g maximum (g being the gravitational acceleration) and a data acquisition system DH5922N (Fig. 3). To overcome the problem, the accelerometers were utilized eight times and the measurement point A_{45} was selected as the stationary location at all time. For example, after the first measurement, the accelerometers were moved from A_{1j} to A_{2j} (j = 1-9). The data acquisition system was used to sample all the results collected from these accelerometers at

Table 1 Thickness and material specification for the steel-bar truss slab

Thickness (mm)	Top bar	Bottom bar	Web bar
120	C10	C8	A4.5

Table 2 Detailed cross sections and yield strength for the H-shaped steel girders

Steel girder number	Cross section (mm)	Yield strength (MPa)
B01	HN175×90×5×8	345
B02	H650×220×10×16	
B03	H500×120×8×10	
B04	H500×150×8×12	
B05	H900×200×10×16	
B06	H650/900/650×240×10×20	

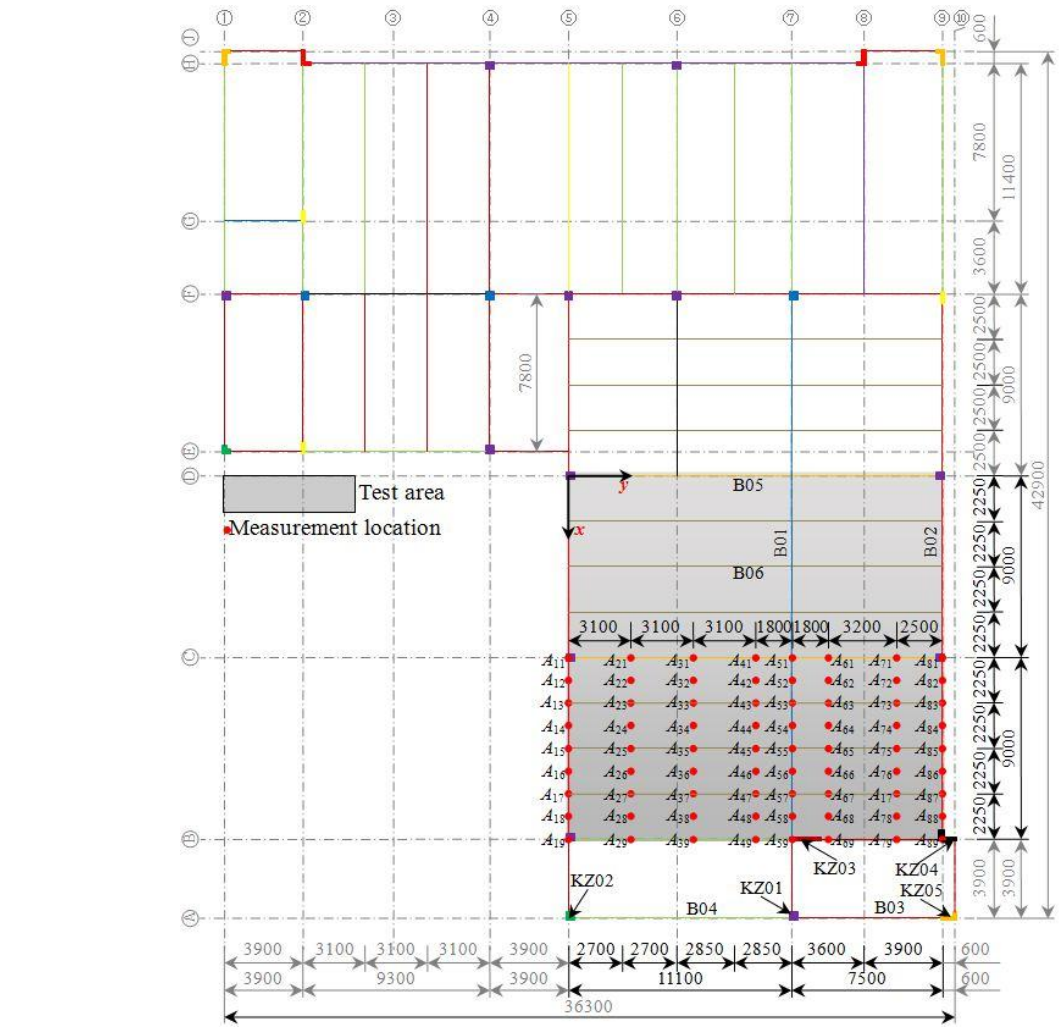

(a) Structural layout and layout of accelerometers

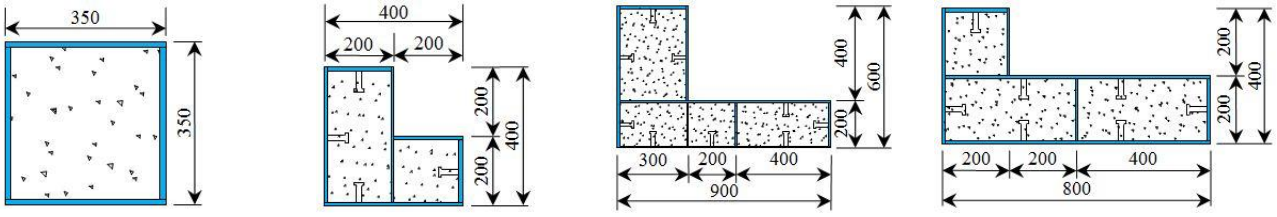

(b) KZ01 (c) KZ02 (d) KZ04 (e) KZ05

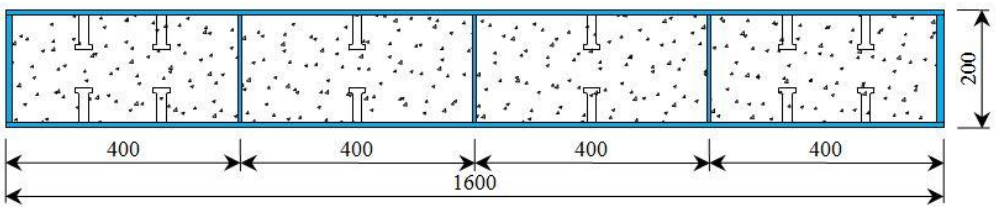

(f) KZ03

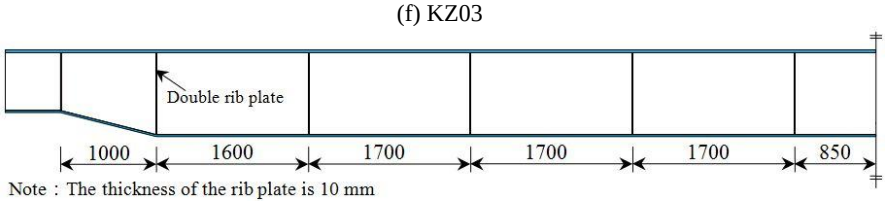

(g) B06

Fig. 2 The structural arrangement and cross section of composite floor and layout of accelerometers (unit: mm)

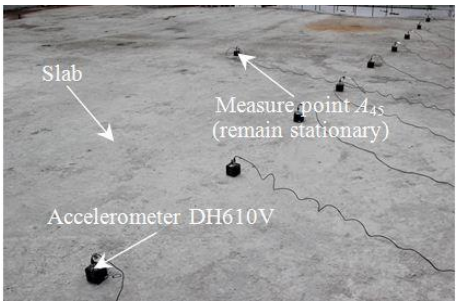

(a) Slab and accelerometers

(b) H-shaped steel girder and baseplate

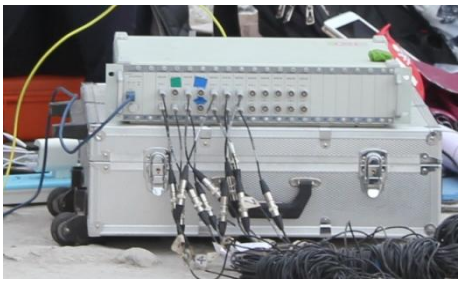

(c) Data acquisition system DH5922N

Fig. 3 The on-site view of CSTS with steel girder and measurement apparatus

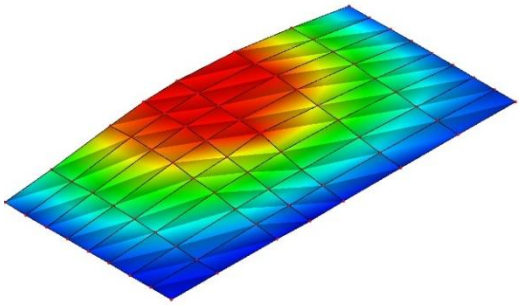

(a) First mode shape

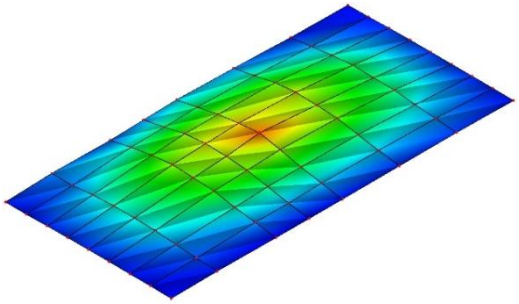

(b) Second mode shape

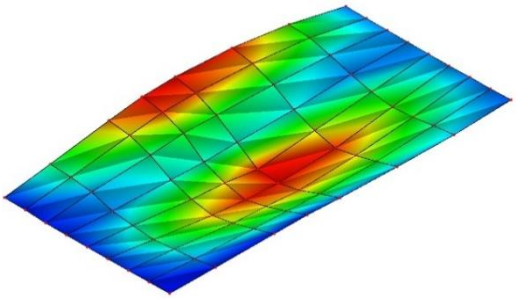

(c) Third mode shape

Fig. 4 The first three mode shapes of composite floor

1000 Hz. Before each formal test procedure, a preloading was performed to determine an appropriate acceleration range for recording the acceleration response.

3. Modal analysis

To ascertain the important parameters of assessing the vibration serviceability, i.e., natural frequency, mode shape, and damping ratio, the ambient vibration method is needed. For an arbitrary row of accelerometers (A_{i1} – A_{i9}, i = 1-8), the duration time is 300s. The enhanced frequency domain decomposition (EFDD) method has been used to processes the test data (Altunisik *et al*. 2011, Pioldi and Rizzi 2018).

The first three vertical mode shapes of the composite floor are shown in Fig. 4 and the measured natural frequencies and damping ratios for the first three vibration modes are summarized in Table 3. As noted, these frequencies are less than 10 Hz, indicating that the composite floor is relatively flexible (Smith *et al*. 2009). The measured critical damping ratio for the composite floor is 2.00% which is consistent with the value suggested by the AISC (Murray *et al*. 2016).

Table 3 Measured natural frequencies and damping ratios of the composite floor for the first three vibrations modes

The *i*th mode	Natural frequencies (Hz)	Damping ratio (%)
1	5.31	2.00
2	6.59	0.50
3	9.46	0.60

4. Boundary conditions

Both numerical and theoretical methods were used to determine a reasonable boundary condition for the composite floor. In the numerical simulation, the entire structural system (Fig. 5) was modeled, in which C3D20 element (20-node quadratic brick) available in ABAQUS program were used and the total number of element is 25484. In the theoretical analysis, the composite floor was idealized as an orthotropic plate (Zhang *et al*. 2017), where the *i*th natural frequency f_i can be determined by the Rayleigh principle (Timoshenko and Woinowsky-Krieger 1959)

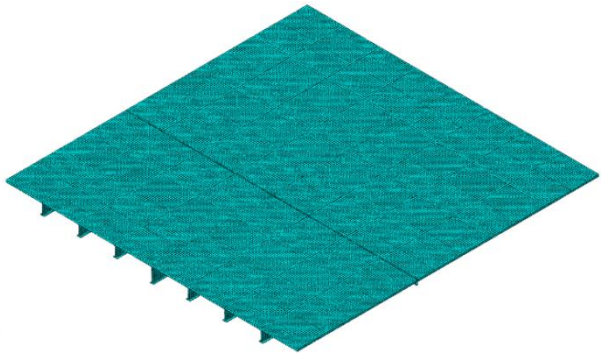

Fig. 5 3D model for the composite floor

Notes: 1. The length of boundary ① and ③ is 18 m;
2. The length of boundary ② and ④ is 18.6 m

Table 4 α_{0i}, α_{1i}, α_{2i}, and α_{3i} coefficients

Boundary condition	i	α_{0i}	α_{1i}	α_{2i}	α_{3i}
CCCC	1	22.373	1.000	1.000	0.605
	2	22.373	7.599	1.000	2.264
	3	22.373	29.204	1.000	5.402
SCSC	1	9.870	5.138	1.000	2.493
	2	9.870	39.047	1.000	9.332
	3	9.870	150.064	1.000	22.270

*Notes: SCSC: two opposite edges simply supported and the other two edges clamped; CCCC: all four edges clamped

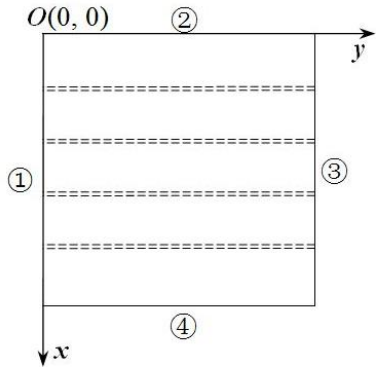

(a) Boundary symbol

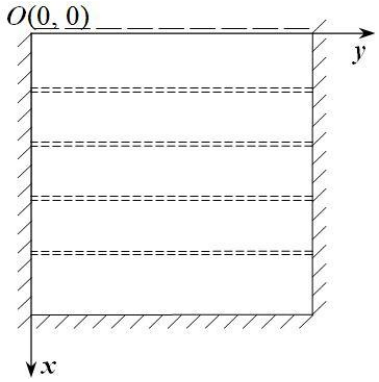

(b) CSCC

Fig. 6 The naming conventions on the boundary condition of the composite floor

$$f_i = \frac{1}{2\pi}\frac{\alpha_{0i}}{b^2}\sqrt{\frac{g}{q_0}}\sqrt{\alpha_{1i}\frac{D_1}{C^4}+\alpha_{2i}D_2+\alpha_{3i}\frac{D_3}{C^2}} \quad (1)$$

where $C = a/b$ with a = plate width and b = beam span; D_1 and D_2 are the plate stiffnesses in x and y directions, respectively; D_3 is the combined rigidity; and q_0 is the weight per unit area of the plate; and α_{0i}, α_{1i}, α_{2i}, and α_{3i} are the coefficients depending on the boundary condition (Table 4). It should be noted that the boundary conditions listed in Table 4 are in accordance with the convention defined in Fig. 6 and that the vibration mode functions for boundary conditions "CC" and "SS" are described in Table 5.

According to the literatures (Smith *et al*. 2009, Timoshenko and Woinowsky-Krieger 1959) and Fig. 2(a), the coefficients D_1, D_2, D_3 and q_0 in Eq. (1) were determined as 4.32×10^6 N·m, 5.01×10^8 N·m, 4.46×10^6 N·m, and 3658.90 N/m^2, respectively. Table 6 lists the first three natural frequencies obtained analytically and numerically under different boundary conditions and the errors with the measured values (Table 3). Considering the beam-slab stiffness ratio and the effect of adjacent structure (Zhou *et al*. 2017), the boundary condition of "CCCC" or "SCSC" was assumed first for the composite floor. The mode shape of the composite floor with SCSC edges are shown in Fig. 7. As noted, under the boundary conditions "CCCC" the error from either the analytical or the finite element method is quite high. While, under the boundary condition "SCSC" the error is relatively small and both methods yield virtually the same results. Consequently, the boundary condition "SCSC" is deemed more reasonable in performing a theoretical or numerical vibration analysis.

Table 5 Vibration mode functions for boundary conditions "CC" and "SS"

Boundary condition		Vibration mode function	k_j			Coefficient γ_j
			1	2	$j>2$	
CC	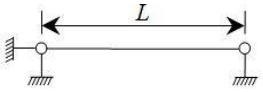	$W_j(z)=\sin k_j z$	$\frac{\pi}{L}$	$\frac{2\pi}{L}$	$\frac{j\pi}{L}$	---
SC	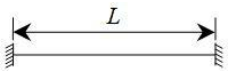	$W_j(z)=\sin k_j z-\sinh k_j z$ $-\gamma_j(\cos k_j z-\cosh k_j z)$	$\frac{4.7300}{L}$	$\frac{7.8532}{L}$	$\frac{(2j+1)\pi}{2L}$	$\frac{\sin k_j L-\sinh k_j L}{\cos k_j L-\cosh k_j L}$

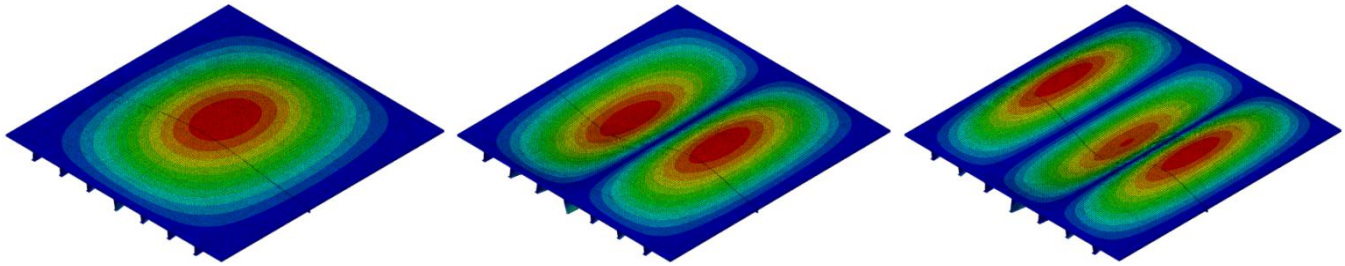

(a) First mode shape (b) Second mode shape (c) Third mode shape

Fig. 7 The first three mode shapes of composite floor with SCSC edges

In order to further illustrate the suitability of boundary condition "SCSC", the modal assurance criterion (MAC) (Eq. (2)) (Xiong *et al*. 2018, Yashar *et al*. 2018) was adopted to analyse the correlation among the experimental, analytical, and numerical mode shapes.

$$\mathrm{MAC}_{ij} = \frac{\left|\phi_i^{\mathrm{T}} \tilde{\phi}_j\right|^2}{(\phi_i^{\mathrm{T}} \phi_i)(\tilde{\phi}_j^{\mathrm{T}} \tilde{\phi}_j)} \tag{2}$$

where ϕ_i and $\tilde{\phi}_j$ represent the ith and jth ($i = j = 1, 2, 3$) experimental and theoretical/numerical mode shapes, respectively.

Table 7 lists the MAC values for the ith mode shape. The table results indicate that both the theoretical and numerical mode shapes agree well with experimental results.

Based on the above analysis, the reasonable boundary condition of SCSC (i.e., two opposite edges simply supported and the other two edges clamped) is confirmed to be reasonable for the composite floor.

Table 6 The analytical and numerical natural frequencies under different boundary conditions and their errors with the measured values

Boundary condition	Method	The ith natural frequency (Hz)			Error with measured value (%)		
		1	2	3	1	2	3
CCCC	Theory	12.0	12.5	13.8	126	89.7	45.9
	FE	9.96	10.6	12.7	87.6	60.5	34.2
SCSC	Theory	5.45	6.38	8.62	2.64	3.19	8.87
	FE	5.53	6.89	9.53	4.14	4.55	0.74

Table 7 MAC values for the ith mode shape

Direction	Method	The ith mode shape		
		1	2	3
A_{11}-A_{81}	Theory	0.987	0.915	0.994
	FE	0.993	0.915	0.994
A_{41}-A_{49}	Theory	0.974	0.974	0.963
	FE	0.973	0.976	0.967

5. Walking excitations

Human-induced vibration could be very complex, involving the magnitude of motion, surrounding environment, and human's perceptibility. A continuous steady-state motion may cause an annoying vibration. So, a series of walking tests were performed to estimate the vertical acceleration response and modal parameters of the

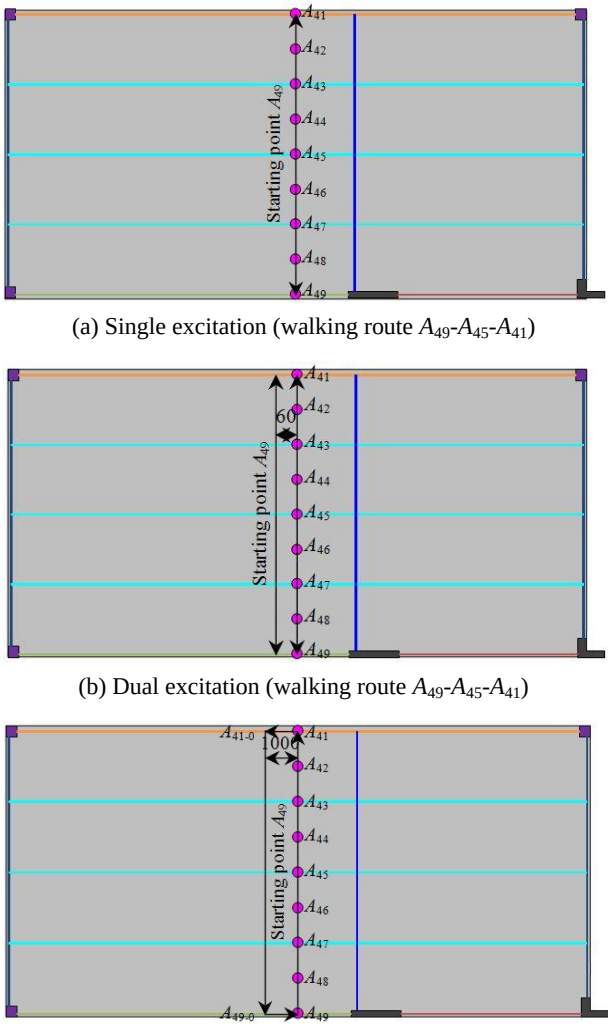

(a) Single excitation (walking route A_{49}-A_{45}-A_{41})

(b) Dual excitation (walking route A_{49}-A_{45}-A_{41})

(c) Triple excitation (walking route A_{49}-A_{45}-A_{41})

Fig. 8 The walking route for triple excitation (route A_{49}-A_{45}-A_{41}, unit: mm)

composite floor. To better understand the vibration performance, the following three forms of steady-state excitations were considered: single excitation (done by one tester), dual excitation (done by two testers), and triple excitation (done by three testers).

(a) Single excitation

(b) Dual excitation

(c) Triple excitation

Fig. 9 The on-site views of walking excitations (mm)

For the single excitation, three different persons weighted at 50 kg (N_{m1}), 56 kg (N_{m2}), and 74 kg (N_{m3}) respectively were considered. Starting from A_{i9} (i = 4, 5, 6), each tester walked along the following routes repeatedly for a duration of 3 minutes: $A_{i9}\rightarrow A_{i5}\rightarrow A_{i1}\rightarrow A_{i5}\rightarrow A_{i9}\rightarrow\ldots$, for example when i = 4, the route is shown in Fig. 8(a). For the dual excitation, the combinations of testers are indicated in Table 9. Starting from A_{i9} (i = 4, 5, 6), two testers spaced at 60 mm walked along the following routes repeatedly for duration of 3 minutes: $A_{i9}\rightarrow A_{i5}\rightarrow A_{i1}\rightarrow A_{i5}\rightarrow A_{i9}\rightarrow\ldots$, for example when i = 4, the route is shown in Table 8(b). For the triple excitation, starting from A_{i9} (i = 4, 5, 6) in turn, each tester spaced 1000 mm from previous tester walked along the following routes repeatedly for a duration of 3 minutes: $A_{i9}\rightarrow A_{i5}\rightarrow A_{i1}\rightarrow A_{i1\text{-}0}\rightarrow A_{i9\text{-}0}\rightarrow A_{i9}\rightarrow\ldots$, and it should be noted that the distance between $A_{i1\text{-}0}$ (or $A_{i9\text{-}0}$) to A_{i1} (or A_{i9}) is 1000 mm, for example when i = 4, the route is shown in Fig. 8(c). Normal walking frequencies were recorded using a video device, Vidicon, as summarized in Tables 8, 9, and 10 for the three kinds of excitation, respectively. The on-site walking tests are shown in Fig. 9.

Table 8 The walking frequencies under single excitation (Hz)

Exciter	Walking route		
	A_{49}-A_{45}-A_{41}	A_{59}-A_{55}-A_{51}	A_{69}-A_{65}-A_{61}
N_{m1}	1.80	1.80	1.80
N_{m2}	1.90	1.90	2.00
N_{m3}	1.80	1.65	1.80

Table 9 The walking frequencies under dual excitation (Hz)

Exciter	Walking route		
	A_{49}-A_{45}-A_{41}	A_{59}-A_{55}-A_{51}	A_{69}-A_{65}-A_{61}
N_{m1} and N_{m2}	1.90	1.80	1.90
N_{m1} and N_{m3}	1.85	1.85	1.85
N_{m2} and N_{m3}	1.90	1.85	1.80

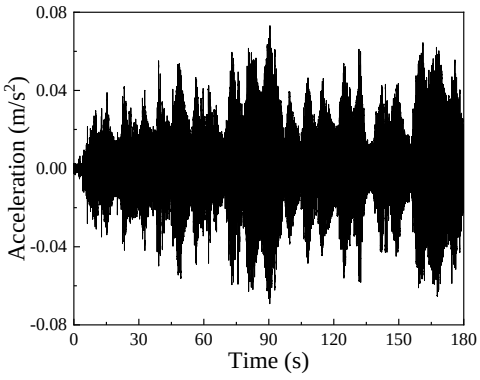

(a) The raw data

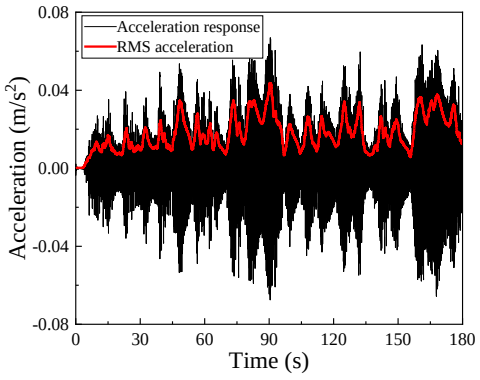

(b) Denoised data

Fig. 10 The acceleration response of the composite floor

Table 10 The walking frequencies under triple excitation (Hz)

Exciter	Walking route		
	A_{49}-A_{45}-A_{41}	A_{59}-A_{55}-A_{51}	A_{69}-A_{65}-A_{61}
N_{m1}, N_{m2} and N_{m3}	1.80	1.80	1.70

5.1 Vibration serviceability evaluation

The response of the composite floor was evaluated in terms of peak and RMS accelerations. Although the peak acceleration is the highest acceleration resulting from an excitation, it gives no indication as to the duration of time that the system is subjected to this level of acceleration. In contrast, the RMS acceleration represents the average measurement of an acceleration-time history, as expressed by Davis *et al*. (2014) and Sa *et al*. (2017)

$$a_{\mathrm{rms}}(t)=\sqrt{\frac{1}{N}\sum_{i=1}^{N}a_i^2(t)} \tag{3}$$

where $a_{\mathrm{rms}}(t)$ is the rolling RMS acceleration at time t; N is the number of acceleration data points measured between t-1 and t+1; and $a_i(t)$ is the ith acceleration data point.

To improve the reliability of the results, Daubechies wavelet method (Jimenez-Alonso *et al*. 2014, Mokhtari and Mirdamadi 2018) was adopted to remove the noise from the raw data. The comparison between the raw and denoised data are shown in Fig. 10. The peak and RMS accelerations (typical example shown in Fig. 10(b)) of the composite floor due to the walking excitations along the various routes are listed in Table 11, 12, and 13, respectively. From these tables, the maximum peak and RMS acceleration are found to be approximately equal to 17.26×10^{-2} m/s^2 (= 1.76%g) and 6.48×10^{-2} m/s^2 (= 0.66%g), respectively. All the RMS accelerations indicated in Tables 11-13 are below the vibration acceptability limit of 1.5%g specified in the AISC (Murray *et al*. 2016).

Table 11 The peak and RMS accelerations at each measuring point along route A_{41}-A_{49} ($\times10^{-2}$m/s^2)

Measure point		Single			Dual			Triple
		N_{m1}	N_{m2}	N_{m3}	N_{m1} and N_{m2}	N_{m1} and N_{m3}	N_{m2} and N_{m3}	
A_{41}	Peak	3.67	5.76	5.34	7.17	6.85	7.71	6.80
	RMS	1.10	1.49	1.89	2.97	2.58	3.67	3.47
A_{42}	Peak	3.48	5.22	6.14	6.47	11.15	7.11	7.35
	RMS	1.30	1.48	3.02	2.68	2.63	3.21	3.56
A_{43}	Peak	3.43	8.14	7.72	5.26	11.76	5.49	8.68
	RMS	1.47	2.21	4.73	2.17	2.38	3.00	5.15
A_{44}	Peak	4.17	9.63	8.91	4.52	13.46	5.56	10.16
	RMS	1.54	1.78	5.73	2.00	3.33	2.90	6.36
A_{45}	Peak	3.46	6.97	8.22	4.66	8.34	5.32	11.69
	RMS	1.34	1.45	5.41	2.07	2.03	2.48	5.98
A_{46}	Peak	4.65	8.01	7.74	4.93	12.61	6.60	**17.26**
	RMS	1.17	1.70	4.96	2.36	2.60	2.88	5.44
A_{47}	Peak	2.86	5.04	5.32	4.95	6.54	4.97	7.55
	RMS	0.74	1.28	3.17	2.57	1.74	2.27	3.47
A_{48}	Peak	6.35	5.60	5.85	3.25	12.82	4.66	10.1
	RMS	1.13	1.74	1.59	1.04	2.72	1.27	1.86
A_{49}	Peak	5.99	6.30	3.44	2.09	8.23	2.02	2.67
	RMS	0.65	1.85	0.44	0.23	1.57	0.35	0.32

Table 12 The peak and RMS accelerations at each measuring point along route A_{51}-A_{59} ($\times10^{-2}$m/s^2)

Measure point		Single			Dual			Triple
		N_{m1}	N_{m2}	N_{m3}	N_{m1} and N_{m2}	N_{m1} and N_{m3}	N_{m2} and N_{m3}	
A_{45}	Peak	3.10	3.45	8.89	6.10	7.76	7.61	10.43
	RMS	1.56	1.39	5.80	2.98	3.97	3.76	**6.48**
A_{51}	Peak	2.37	3.87	5.14	3.60	4.50	6.12	7.08
	RMS	1.16	1.39	2.03	1.66	2.39	2.79	2.46
A_{52}	Peak	2.26	3.73	5.09	4.03	4.87	5.49	5.92
	RMS	1.18	1.33	2.33	1.97	2.54	2.45	2.71
A_{53}	Peak	2.63	2.84	6.41	4.74	5.04	5.52	9.26
	RMS	1.26	0.99	3.86	2.38	2.86	2.67	4.42
A_{54}	Peak	2.61	3.13	7.27	4.97	5.91	5.89	8.50
	RMS	1.33	1.08	4.63	2.53	3.24	2.93	5.21
A_{55}	Peak	2.35	2.66	6.75	4.54	5.82	5.72	7.79
	RMS	1.18	1.05	4.38	2.25	2.99	2.85	4.88
A_{56}	Peak	3.18	3.34	7.97	4.13	5.48	6.03	8.46
	RMS	1.05	1.14	3.95	2.04	2.70	2.75	4.41
A_{57}	Peak	2.04	2.47	4.83	3.21	4.03	4.99	5.42
	RMS	0.68	0.93	2.52	1.32	1.73	2.06	2.83
A_{58}	Peak	2.17	3.01	3.86	2.59	2.98	2.79	3.83
	RMS	0.34	0.71	1.21	0.64	0.88	1.10	1.37
A_{59}	Peak	1.24	2.31	1.69	1.01	0.81	1.18	4.71
	RMS	0.10	0.20	0.16	0.21	0.14	0.12	0.31

Table 13 The peak and RMS accelerations at each measuring point along route A_{61}-A_{69} ($\times10^{-2}$m/s^2)

Measure point		Single			Dual			Triple
		N_{m1}	N_{m2}	N_{m3}	N_{m1} and N_{m2}	N_{m1} and N_{m3}	N_{m2} and N_{m3}	
A_{45}	Peak	3.10	3.20	9.47	5.75	6.53	6.40	9.81
	RMS	1.39	1.72	6.22	2.50	3.78	3.71	6.43
A_{61}	Peak	2.20	2.07	4.10	3.71	4.62	4.24	5.52
	RMS	0.76	0.95	1.17	1.46	1.60	1.59	1.91
A_{62}	Peak	2.56	2.32	5.05	4.23	4.85	4.10	4.68
	RMS	0.81	0.97	2.23	1.55	1.82	1.80	2.10
A_{63}	Peak	2.53	2.07	5.60	3.51	4.08	4.11	5.68
	RMS	0.88	1.03	3.57	1.75	2.26	2.19	3.60

Table 13 Continued

Measure point		Single			Dual			Triple
		N_{m1}	N_{m2}	N_{m3}	N_{m1} and N_{m2}	N_{m1} and N_{m3}	N_{m2} and N_{m3}	
A_{64}	Peak	2.32	2.37	6.95	4.13	4.98	5.03	6.79
	RMS	0.96	1.20	4.30	1.84	2.65	2.58	4.44
A_{65}	Peak	2.22	2.19	6.45	3.82	4.75	4.04	6.45
	RMS	0.94	1.12	4.03	1.63	2.43	2.40	4.16
A_{66}	Peak	2.45	3.07	5.97	4.42	4.81	4.18	6.69
	RMS	0.91	1.01	3.59	1.43	2.14	2.16	3.72
A_{67}	Peak	2.41	2.20	3.94	4.12	4.07	3.50	4.55
	RMS	0.69	0.66	2.28	1.00	1.37	1.40	2.37
A_{68}	Peak	2.24	1.76	4.03	3.67	4.63	3.02	3.00
	RMS	0.48	0.38	1.12	0.68	0.75	0.73	1.20
A_{69}	Peak	0.13	1.42	1.34	1.04	2.87	1.54	0.53
	RMS	0.03	0.13	0.35	0.19	0.31	0.25	0.12

Table 14 β_{rp} factors corresponding to the walking on the composite floor along route A_{41}-A_{49}

Measure point	Single			Dual			Triple
	N_{m1}	N_{m2}	N_{m3}	N_{m1} and N_{m2}	N_{m1} and N_{m3}	N_{m2} and N_{m3}	
A_{41}	3.34	3.87	2.83	2.41	2.66	2.10	1.96
A_{42}	2.68	3.53	2.03	2.41	4.24	2.21	2.06
A_{43}	2.33	3.68	1.63	2.42	4.94	1.83	1.69
A_{44}	2.71	5.41	1.55	2.26	4.04	1.92	1.60
A_{45}	2.58	4.81	1.52	2.25	4.11	2.15	1.95
A_{46}	3.97	4.71	1.56	2.09	4.85	2.29	3.17
A_{47}	3.86	3.94	1.68	1.93	3.76	2.19	2.18
A_{48}	5.62	3.22	3.68	3.13	4.71	3.67	5.43
A_{49}	9.22	3.41	7.82	9.09	5.24	5.77	8.34

5.2 Crest factor β_{rp}

The RMS acceleration is usually used to assess the vibration serviceability (Murray *et al*. 2016). The determination of RMS accelerations involves a tedious calculation process which is inconvenient to engineers. This study proposes a crest factor β_{rp}, as describing by Eq. (4), to facilitate the calculation of RMS accelerations.

$$\beta_{rp} = \frac{a_{Peak}}{a_{rms}} \tag{4}$$

Based on the Grubbs' criterion contained in GB/T 4883-2008 (2008), individual β_{rp} factors and the average value under a detection level α_{lev} = 0.05 can be obtained, as summarized in Tables 14-17. For design convenience and safety, β_{rp} = 2.03 is suggested.

Table 15 β_{rp} factors corresponding to the walking on the composite floor along route A_{51}-A_{59}

Measure point	Single			Dual			Triple
	N_{m1}	N_{m2}	N_{m3}	N_{m1} and N_{m2}	N_{m1} and N_{m3}	N_{m2} and N_{m3}	
A_{45}	1.99	2.48	1.53	2.05	1.95	2.02	1.61
A_{51}	2.04	2.78	2.53	2.17	1.88	2.19	2.88
A_{52}	1.92	2.80	2.18	2.05	1.92	2.24	2.18
A_{53}	2.09	2.87	1.66	1.99	1.76	2.07	2.10
A_{54}	1.96	2.90	1.57	1.96	1.82	2.01	1.63
A_{55}	1.99	2.53	1.54	2.02	1.95	2.01	1.60
A_{56}	3.03	2.93	2.02	2.02	2.03	2.19	1.92
A_{57}	3.00	2.66	1.92	2.43	2.33	2.42	1.92
A_{58}	6.38	4.24	3.19	4.05	3.39	2.54	2.80

Table 16 β_{rp} factors corresponding to the walking on the composite along route A_{61}-A_{69}

Measure point	Single			Dual			Triple
	N_{m1}	N_{m2}	N_{m3}	N_{m1} and N_{m2}	N_{m1} and N_{m3}	N_{m2} and N_{m3}	
A_{45}	2.23	1.86	1.52	2.30	1.73	1.73	1.53
A_{61}	2.89	2.18	3.50	2.54	2.89	2.67	2.89
A_{62}	3.16	2.39	2.26	2.73	2.66	2.28	2.23
A_{63}	2.88	2.01	1.57	2.01	1.81	1.88	1.58
A_{64}	2.42	1.98	1.62	2.24	1.88	1.95	1.53
A_{65}	2.36	1.96	1.60	2.34	1.95	1.68	1.55
A_{66}	2.69	3.04	1.66	3.09	2.25	1.94	1.80
A_{67}	3.49	3.33	1.73	4.12	2.97	2.50	1.92
A_{68}	4.67	4.63	3.60	5.40	6.17	4.14	2.50

Table 17 Average β_{rp} factors for different walking excitations on the composite floor

Single excitation	Dual excitation	Triple excitation
2.74	2.79	2.03

6. Effect of human-structure interaction

The modal parameters of the composite floor can also be determined by the walking excitations. The natural frequencies and damping ratios determined by the walking excitations are listed in Table 18. Comparisons of the mode shapes obtained by the ambient vibration and walking tests are presented in Figs. 11-13. The table and figures show that the modal parameters determined by the ambient vibration and walking excitations are not exactly the same. Some significant differences are noted. The main reason for this is that the walk behaviour of a person will influence the vibration characteristics of a long span and light-weight floor (Shahabpoor *et al*. 2016), i.e., having the effect of human-structure interaction.

Table 18 Modal properties of the composite floor under different excitations

The ith modal parameter		Single			Dual			Triple
		N_{m1}	N_{m2}	N_{m3}	N_{m1} and N_{m2}	N_{m1} and N_{m3}	N_{m2} and N_{m3}	
Frequency (Hz)	1	5.31	5.37	5.28	5.37	5.31	5.31	5.19
	2	6.56	6.56	6.56	6.56	6.56	6.56	6.56
	3	9.46	9.37	9.43	9.43	9.40	9.43	9.31
Damping ratio (%)	1	1.00	2.60	2.00	1.10	2.00	1.20	2.10
	2	0.40	0.5	1.00	0.80	1.20	0.40	0.50
	3	0.90	1.30	0.80	0.40	2.00	0.90	2.00

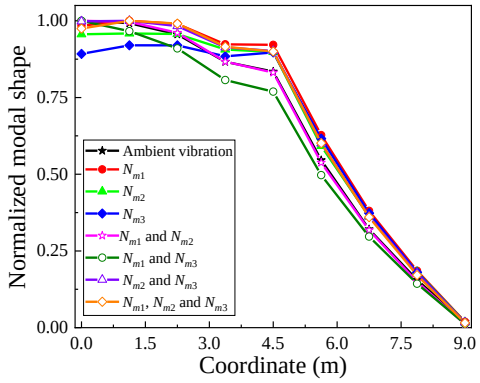

(a) A_{41}-A_{49}

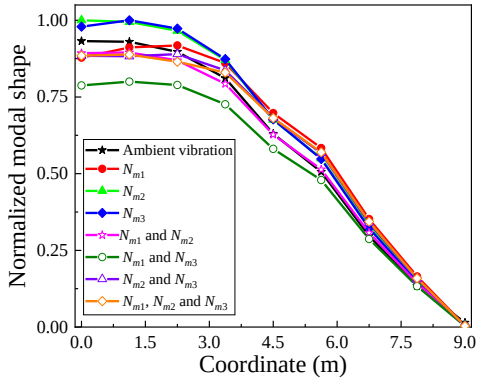

(b) A_{51}-A_{59}

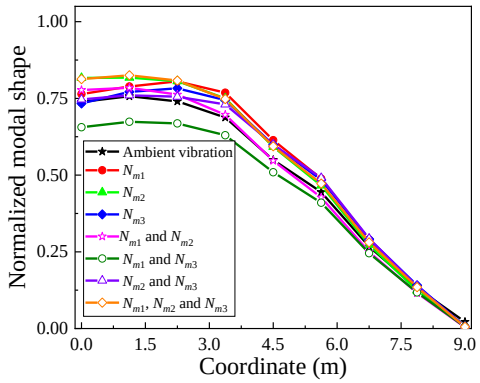

(c) A_{61}-A_{69}

Fig. 11 Comparison of the first vertical mode shapes for the composite floor under different excitations

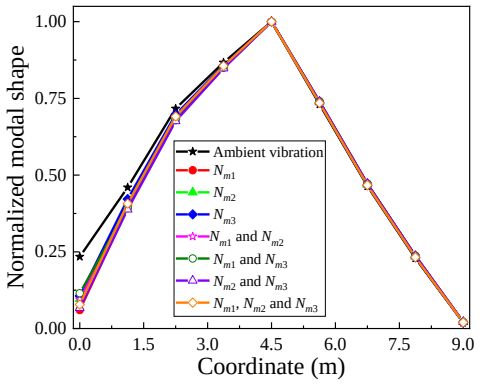

(a) A_{41}-A_{49}

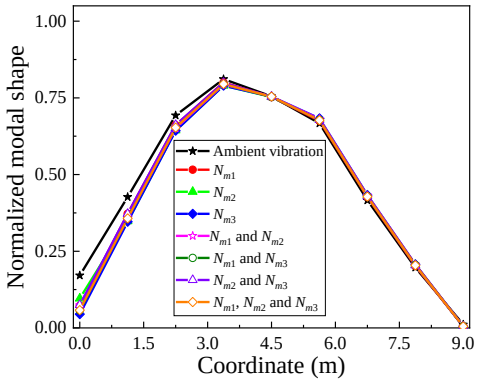

(b) A_{51}-A_{59}

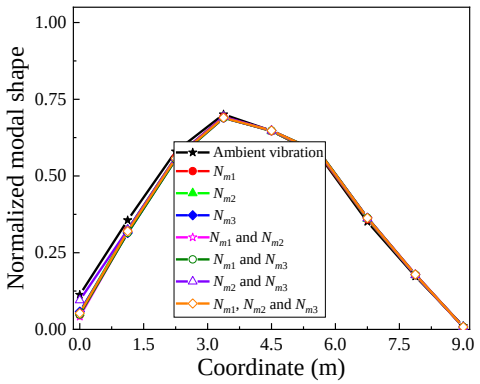

(c) A_{61}-A_{69}

Fig. 12 Comparison of the second vertical mode shapes for the composite floor under different excitations

7. Influence factor of interaction effect

To discuss the influence of sectional dimension on interaction effect, theoretical methods were used. Detailed derivation process for the analytical solution are shown in literature Cao 2017. The cross section of composite floorconsidered in this section are the same as the investigated floor shown in Fig. 2, and only the length and span (listed in Table 19) are changed. The acceleration induced be walking with interaction and without it are listed in Table 20. From the table, it demonstrates that the interaction effect will increase the acceleration response, and with the increasing stiffness of the composite floor, the interaction effect gradually decreases.

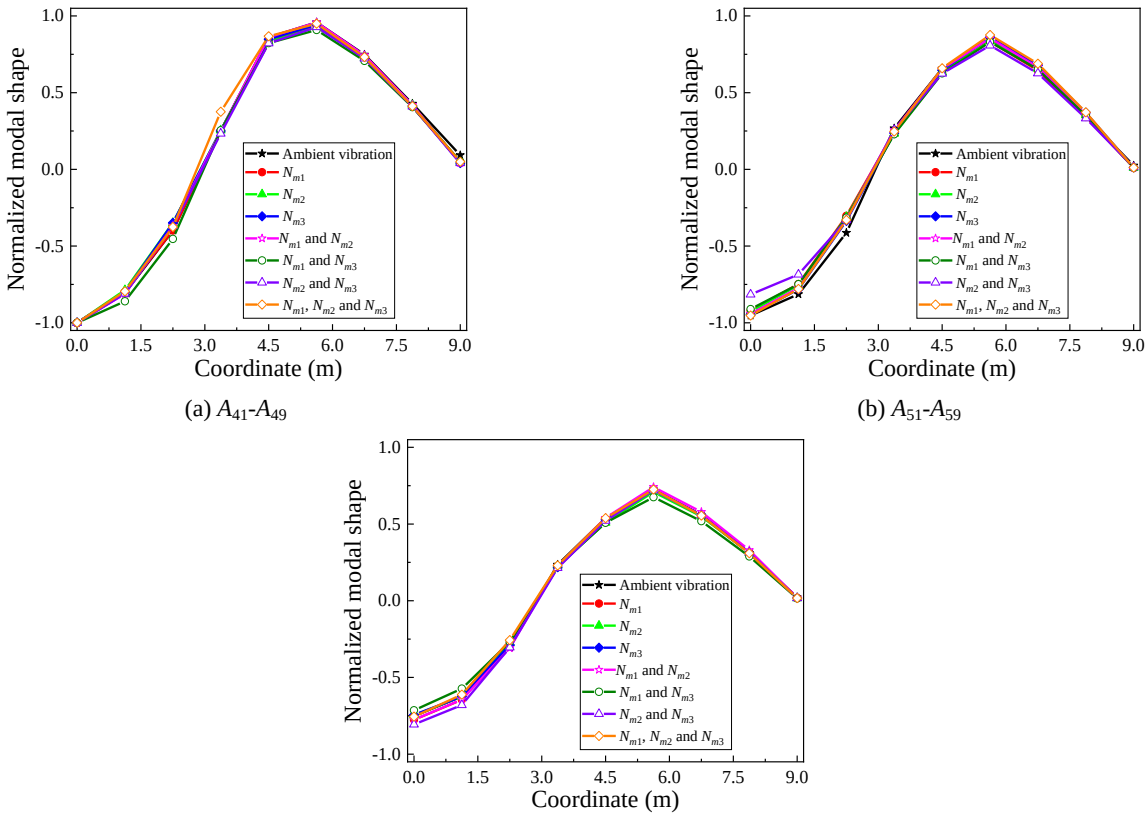

(a) A_{41}-A_{49} (b) A_{51}-A_{59}

(c) A_{61}-A_{69}

Fig. 13 Comparison of the third vertical mode shapes for the composite floor under different excitations

Table 19 The structure parameters of the composite floor

Length (m)	18	22.5	27
Span (m)	18	18	18
Uniform load (N/m^2)	3481.3	3496.48	3506.79
Natural frequency f_1 (Hz)	5.61	5.50	5.45

Table 20 The peak acceleration of the composite floor with interaction and without it

Length (m)		18	22.5	27
Span (m)		18	18	18
Peak acceleration ($\times10^{-2}$m/s^2)	Interaction	4.40	3.00	2.10
	Non-interaction	4.14	2.80	1.93
RMS ($\times10^{-2}$m/s^2)	Interaction	1.58	1.08	0.75
	Non-interaction	1.48	1.00	0.69
Error (%)		5.90	6.67	8.10

8. Conclusions

A comprehensive research was undertaken to study the vibration performance of the composite steel-bar truss slab (CSTS) with steel girder, where the ambient vibration and walking tests (single, dual, and triple excitations) were conducted on-site. Based on the study results, the following primary findings and conclusions are offered:

- The first three natural frequencies of the composite floor are 5.31 Hz, 6.59 Hz, and 9.46 Hz, indicating that the composite floor is relatively flexible since these frequencies are all under the recommended practical value of 10 Hz. The damping ratios for the first three vibration modes of the composite floor are 2.00%, 0.50%, and 0.60%, all below the AISC suggested limit of 2.00% for bare floors.
- The natural frequencies of the composite floor obtained from the theoretical or numerical method are very different from the experimental results for the boundary condition CCCC (i.e., all four edges clamped), while they are relatively close to each other for the boundary condition SCSC (i.e., two opposite edges simply supported and the other two edges clamped). The minimum MAC (modal assurance criterion) value for the boundary condition SCSC between theoretical/numerical and experimental mode shapes is 0.915. Hence, the boundary condition SCSC is recommended for studying the vibration behavior of the composite floor.
- All obtained RMS accelerations due to walking appear to satisfy the AISC vibration criterion since the maximum value is 0.66%g.
- For design convenience and safety, the crest factor β_{rp} (ratio of peak to RMS accelerations) can be set at 2.03.
- The comparisons of modal parameters among the ambient vibration and walking tests (single, dual,

and triple excitations) show that the walking behavior of a person will influence the vibration characteristics of a long span and light-weight floor, i.e., having the effect of human-structure interaction.
- Interaction effect will increase the acceleration response, and with the increasing stiffness of the composite floor, the interaction effect gradually decreases.

Acknowledgments

The authors are grateful to the supports provided by the National Natural Science Foundation of China (Grant No. 51622802, 51438001) and National Key Research and Development Program of China (Project No. 2016YFC0701201).

References

Altunisik, A.C., Bayraktar, A., Sevim, B. and Ozdemir, H. (2011), "Experimental and analytical system identification of Eynel arch type steel highway bridge", *J. Constr. Steel Res.*, **67**(12), 1912-1921.

Cao, L. (2017), Analytical and experimental studies on the acceleration response of floors induced by human activities, Chongqing University, Chongqing, China. [In Chinese]

Chen, J., Yan, S.X. and Zhang, M.S. (2014), "Vibration performance assessment of a long-span concrete floor using filed measurement over a five-year period", *Adv. Struct. Eng.*, **17**, 1145-1158.

Cheng, J.Y., Zhao, L. and Yang, J.J. (2013), "Study on short-term rigidity of precast composite slab with steel truss and concrete", *Adv. Mater. Res.*, **639-640**, 198-205.

Colajanni, P., Mendola, L.L., Latour, M., Monaco, A. and Rizzano, G. (2017), "Analytical prediction of the shear connection capacity in composite steel-concrete trussed beams", *Mater. Struct.*, **50**(1), 48.

Davis, B., Liu, D. and Murray, T.M. (2014), "Simplified experimental evaluation of floors subject to walking induced vibration", *J. Perform. Constr. Fac.*, **28**(5), 04014023.

Fahmy, Y.G.M. and Sidky, A.N.M. (2012), "An experimental investigation of composite floor vibration due to human activities. A case study", *HBRC Journal*, **8**, 228-238.

Ferrer, M., Marimon, F. and Casafont, M. (2018), "An experimental investigation of a new perfect bond technology for composite slabs", *Constr. Build. Mater.*, **166**, 618-633.

GB/T 4883-2008 (2008), Statistical interpretation of data-Detection and treatment of outliers in the normal sample; Beijing, China.

Gonilha, J.A., Barros, J., Correia, J.R., Sena-Cruz, J., Branco, F.A., Ramos, L.F., Gonçalves, D., Alvim, M.R. and Santos, T. (2014), "Static, dynamic and creep behaviour of a full-scale GFRP-SFRSCC hybrid footbridge", *Compos. Struct.*, **118**, 496-509.

Gou, H., Wang, W., Shi, X., Pu, Q. and Kang, R. (2018), "Behavior of steel-concrete composite cable anchorage system", *Steel Compos. Struct., Int. J.*, **26**(1), 115-123.

Hadjioannou, M., Donahue, S., Williamson, E.B. and Engelhardt, M.D. (2018), "Large-scale experimental tests of composite steel floor systems subjected to column loss scenarios", *J. Struct. Eng.*, **144**(2), 04017184.

Huang, L., Niitani, K. and Hikosaka, H. (2005), "Nonlinear analysis and tests of prestressed concrete composite girders with steel truss webs", *Proceedings of the 10th International Conference on Civil, Structural and Environmental Engineering Computing*, Rome, Italy, May.

JG/T 368-2012 (2012), Steel-bars truss deck; Ministry of Housing and Urban-Rural Development of the People's Republic of China; Beijing, China.

Jimenez-Alonso, J.F., Saez, A., Caetano, E. and Cunha, A. (2014), "Proposal and calibration of an human-structure interation biomechanical model by the resolution of the inverse dynamic problem", *Proceedings of the 9th International Conference on Structural Dynamic*, EURODYN, Porto, Portugal, June.

Kataoka, M.N., Friedrich, J.T. and Debs, A.L.H.C.E. (2017), "Experimental investigation of longitudinal shear behavior for composite floor slab", *Steel Compos. Struct., Int. J.*, **23**(3), 351-362.

Kimani, S.K. and Kaewunruen, S. (2017), "Free vibrations of precast modular steel-concrete composite railway track slabs", *Steel Compos. Struct., Int. J.*, **24**(1), 113-128.

Kyvelou, P., Gardner, L. and Nethercot, D.A. (2018), "Finite element modelling of composite cold-formed steel flooring systems", *Eng. Struct.*, **158**, 28-42.

Li, Y.X., Jiang, L., Yu, Z.Q., Li, J. and Li, Y.W. (2012), "Test research on the behaviors of steel bar truss and concrete superimposed floor slabs", *Appl. Mech. Mater*, **166-169**, 3-8.

Madrazo-Aguirre, F., Ruiz-Teran, A.M. and Wadee, M.A. (2015), "Dynamic behaviour of steel-concrete composite under-deck cable-stayed bridges under the action of moving loads", *Eng. Struct.*, **103**, 260-274.

Mokhtari, A. and Mirdamadi, H.R. (2018), "Study on vibration and stability of an axially translating viscoelastic Timoshenko beam: Non-transforming spectral element analysis", *Appl. Math. Model.*, **56**, 342-358.

Murray, T.M., Allen, D.E., Ungar, E.E. and Davis, D.B. (2016), *Vibrations of Steel-Framed Structural Systems Due to Human Activity*, (2nd Edition), American Institute of Steel Construction, Inc., Chicago, IL, USA.

Nguyen, T.H., Gad, E.F., Wilson, J.L. and Haritos, N. (2012), "Improving a current method for predicting walking-induced floor vibration", *Steel Compos. Struct., Int. J.*, **13**(2), 139-155.

Pioldi, F. and Rizzi, E. (2018), "Assessment of frequency versus time domain enhanced technique for response-only modal dynamic identification under seismic excitation", *B. Earthq. Eng.*, **16**(3), 1547-1570.

Quang, K.M., Park, A., Nguyen, K.T. and Lee, K. (2018), "Full-scale static and dynamic experiments of hybrid CLT-concrete composite floor", *Constr. Build. Mater.*, **170**, 55-65.

Sa, M.F., Guerreiro, L., Gomes, A.M., Correia, J.R. and Silvestre, N. (2017), "Dynamic behaviour of a GFRP-steel hybrid pedestrian bridge in serviceability conditions. Part 1: Experimental study", *Thin-Wall. Struct.*, **117**, 332-342.

Shahabpoor, E., Pavic, A. and Racic, V. (2016), "Identification of mass-spring-damper model of walking humans", *Struct.*, **5**, 233-246.

Smith, A.L., Hicks, S.J. and Devine, P.J. (2009), *Design of Floors for Vibration: A New Approach*, The Steel Construction Institute, Ascot, Berkshire, UK.

Timoshenko, S. and Woinowsky-Krieger, S. (1959), *Theory of Plates and Shells*, Mcgraw-Hill College, New York, USA.

Van Nimmen, K., Van den Broeck, P., Verbeke, P., Schauvliege, C., Mallie, M., Ney, L. and De Roeck, G. (2017), "Numerical and experimental analysis of the vibration serviceability of the Bears' Cage footbridge", *Struct. Infrastruct. E.*, **13**(3), 390-400.

Votsis, R.A., Stratford, T.J., Chryssanthopoulos, M.K. and Tantele, E.A. (2017), "Dynamic assessment of a FRP suspension footbridge through field testing and finite element modelling", *Steel Compos. Struct., Int. J.*, **23**(2), 205-215.

Wang, Y.C. (2005), "Performance of steel-concrete composite

structures in fire", *Prog. Struct. Eng. Mat.*, **7**(2), 86-102.
Wang, W.Y., Li, G.Q., Chen, L.Z., Jiang, S.C. and Huang, G.S. (2015), "Experimental study on fire resistance of steel bar truss slab and steel composite beams", *Chin. Civil Eng. J.*, **48**(9), 67-75.
Wang, Q.H., Ranzi, G., Wang, Y.Y. and Geng, Y. (2016), "Long-term behaviour of simply-supported steel-bars truss slabs with recycled coarse aggregate", *Constr. Build. Mater.*, **116**, 335-346.
Wang, J.F., Li, B.B., Wang, D.H. and Zhao, C.F. (2017a). "Cyclic testing of steel beam blind bolted to CFST column composite frames with SBTD concrete slabs", *Eng. Struct.*, **148**, 293-311.
Wang, J.F., Pan, X.B. and Peng, X. (2017b), "Pseudo-dynamic tests of assembly blind bolted composite frames to CFST columns", *J. Conctr. Steel Res.*, **139**, 83-100.
Xiong, W., Kong, B., Tang, P.B. amd Ye, J.S. (2018), "Vibration-based identification for the presence of scouring of cable-stayed bridges", *J. Aerosp. Eng.*, **31**(2), 04018007.
Yashar, A., Ferguson, N. and Ghandchi-Tehrani, M. (2018), "Simplified modelling and analysis of a rotating Euler-Bernoulli beam with a single cracked edge", *J. Sound Vib.*, **420**, 346-356.
Zhang, S.G., Xu, L. and Qin, J.W. (2017), "Vibration of lightweight steel floor systems with occupants: Modelling, formulation and dynamic properties", *Eng. Struct.*, **147**, 652-665.
Zhou, X.H., Cao, L., Chen, Y.F., Liu, J.P. and Li, J. (2016), "Experimental and analytical studies on the vibration serviceability of pre-stressed cable RC truss floor systems", *J. Sound Vib.*, **361**, 130-147.
Zhou, X.H., Liu, J.P., Cao, L. and Li, J. (2017), "Vibration serviceability of pre-stressed concrete floor system under human activity", *Struct. Infrastruct. E.*, **13**(8), 967-977.

BU